(Proposal to Jefferson Lab PAC-27)

Parity Violating Electron Scattering in the Resonance Region (Res-Parity)

December 6, 2004

W. Boeglin, P. Markowitz
Florida International University, Miami, FL, 33199

C. Keppel
Hampton University, Hampton, VA 23668

G. Niculescu, I. Niculescu
James Madison University, Harrisonburg, VA 22807

P.E. Bosted[1] (spokesperson), V. Dharmawardane (co-spokesperson), R. Ent,
D. Gaskell, J. Gomez, M. Jones, D. Mack, R. Michaels, J. Roche, B. Wojtsekhowski
Jefferson Lab, Newport News, VA 23606

T. Forest, N. Simicevic, S. Wells
Louisiana Tech University, Ruston, LO 71272

K. Kumar, K. Paschke
University of Massachusetts, Amherst, MA 01003

F. R. Wesselmann
Norfolk State University, Norfolk, VA

Yongguang Liang, A. Opper
Ohio University, Athens, Ohio 45701

P. Decowski
Smith College, Northampton, MA 01063

R. Holmes, P. Souder
University of Syracuse, Syracuse, NY 13244

S. Connell, M. Dalton
University of Witwatersrand, Johannesburg, South Africa

R. Asaturyan, H. Mkrtchyan (co-spokesperson), T. Navasardyan, V. Tadevosyan
Yerevan Physics Institute, Yerevan, Armenia

Abstract

We propose to perform the first measurements of the parity violation (PV) asymmetries A_p and A_d over the full resonance region ($1 < W < 2.2$ GeV) at $Q^2 \approx 0.4$ and 1 GeV^2. The measurements consist of scattering 4 and 6 GeV longitudinally polarized

[1]Email: bosted@jlab.org

electrons from unpolarized hydrogen and deuterium targets at a scattering angle centered on 11 degrees. The projected total errors on A_p and A_d are approximately 4% (relative) in each of four regions in W. The overall error is projected to be 3% for each target (equal statistical and systematic errors), while the error on the ratio A_p/A_d is projected to be 3% (dominated by statistical errors).

The goals include searching for resonance structure in A_p and A_d, and exploring both global and local quark-hadron duality with the previously un-studied combination of structure functions probed by PV inelastic electron scattering. The PV asymmetry is particularly sensitive to the isospin decomposition, as well as the axial hadronic current. The results are of great practical importance in more accurately modeling neutrino interactions in the few GeV region, which is essential in the interpretation of neutrino oscillation experiments. The new data will also help in understanding backgrounds and radiative corrections for other PV experiments.

The experiment will use an 80 μA current longitudinally polarized electron beam in Hall C, impinging on 25 cm LH2 and LD2 targets. Most of the running will be at 6 GeV, with the remainder at 4 GeV. Scattered electrons will be detected in the lead glass blocks in the HMS spectrometer. Lead will be placed between the third and fourth layers so that the fourth layer can be used to measure the asymmetry of pions. The detectors will be read out in flux integration mode for each helicity bucket. We request a total of 10 days of production running and 1 day of checkout and calibrations.

An alternative scenario is presented in which the LH2 part of the experiment runs concurrently with GEP-III (E04-108) and the likely accompanying experiment GEP-2γ (E04-019). Scattered electrons would be focused in a fixed-angle DQD spectrometer similar to the T20 deuteron channel previously used in Hall C. The spectrometer would be at a fixed location, centered on a scattering angle of 9 degrees. In this scenario we request two additional days beyond E04-108 and E04-019 for calibrations of the new spectrometer and additional beam polarization measurements.

Contents

1 Introduction and Motivation

The electromagnetic interaction has proved very successful in probing the structure of the nucleon. Inelastic electron scattering at high momentum transfer Q^2 and excitation energy ν (corresponding to large missing mass W) has provided the best information to date on the parton distribution functions, whose universal nature makes them useful in understanding a wide variety of particle interactions with nucleons. One limitation is that spin-averaged inclusive electron scattering probes quarks weighted by their charge squared: for a proton target this means that the contribution from down and strange quarks is strongly suppressed relative to the up quarks. Our best information on the down quark PDFs come from using a neutron target, although at high momentum fraction $x = Q^2/2M\nu$ (where M is the nucleon mass), corrections from nuclear binding (Fermi motion) become large. Because the weak charges of the strange and down quarks are relatively larger than the electromagnetic ones, the weak interaction can provide another sensitive means to probe the down and strange PDFs.

An alternative basis for the description of nucleon excitations is in terms of transition form factors to specific resonant states. Lately, the subject of quark-hadron duality has received considerable interest, both theoretically and experimentally. Theoretical interest comes about in making a unified QCD description of the hadronic interactions. Experimental interest arises because to the extent that duality works, it can be used to extract both spin-averaged and spin-dependent PDFs at large x. Duality is also of great importance experimentally to predict cross sections in regions where they haven't been measured precisely (for example, in predicting neutrino scattering cross sections needed to interpret neutrino oscillation experiments). The weak neutral current gives access to the the axial hadronic current, which also enters in weak charge current interactions.

Electron scattering measurements sensitive to the weak neutral current are quite limited. The pioneering experiment of Prescott *et al.* [1] using inelastic scattering on the deuteron helped establish the standard electroweak model. The relatively large errors on the parity-violating asymmetry A_d measured in this experiment are no longer relevant in constraining physics beyond the Standard Model, or in constraining the strange quark PDFs. The experimental program at HERA at very high Q^2 (comparable to M_Z^2, where M_Z is the Z-boson mass) are of limited statistical precision. Most electron PV experiments have focused on elastic channels, with the goal of probing the strange quark form factor of the nucleon (SAMPLE at Bates, HAPPEX and G0 at JLab, A4 at Mainz, etc.), and ultimately searching for physics beyond the standard Model (QWeak at JLab). While experiments such as G0 plan to study the $N - \Delta$ transition, there are presently no approved experiments to extend PV inelastic electron scattering into the full resonance region ($W < 2.2$ GeV) and beyond into the DIS region. With an 11 GeV electron beam at JLab, or a 30 GeV beam at SLAC, it will be possible to repeat the original Prescott experiment with more than an order-of-magnitude reduction in error bars. This will allow a competitive search for new physics, or to establish coupling of new particles if they have already been found at LHC. One hint that such new physics may exist comes from the observation of a 3-sigma discrepancy with the Standard Model from the NuTeV neutrino scattering experiment at Fermilab [2]. Conventional explanations also exist, for example a particle-antiparticle asymmetry in the strange sea, charge symmetry violation, or higher twist corrections.

The interpretation of a new high-precision electron scattering experiment will rely on a reasonable understanding of scattering at lower energy and W, through radiative effects. If a given experiment measures electron scattering with incident energy E_0 and scattered electron energy E_0', the helicity-dependent cross sections must be known at all energies $E > E_0'$ and all $E_0' < E' < E_0$. For $E_0 = 11$ GeV, E_0' will typically be 3 to 5 GeV (see JLab 12 GeV pCDR), so measurements are needed down to $E = 3$ GeV.

Lower energy data will also be crucial to understand the role of higher twist corrections, which are generally expected to decrease with powers of Q^2 and/or W^2. Measurements over a large range of Q^2 and W are needed to measure higher twist diagrams, because there are no models to calculate them reliably.

Another motivation for this proposal comes from the desire to understand backgrounds in other PV experiments. In the recently completed E158 experiment [4] at SLAC, the primary electron-electron (Møller) scattering signal was mixed with electron-proton scattering background, enhanced through radiative effects by the relatively long 180 cm LH2 target. While the *ep* elastic contributions are relatively well understood, the inelastic contribution (with an asymmetry about 20 times larger than the Møller asymmetry), turned out to generate the largest systematic error of this experiment. While measurements were made in a special detector that measured only *ep* scattering, the W-range was quite different than that of the Møller detectors, and elastic and inelastic contributions were strongly mixed. Dedicated measurements of the W dependence of PV inelastic scattering will help reduce the systematic error on the E158 result, which is at present one of the three most precise Standard Model tests away from the Z-pole.

The study of the resonance region is also of interest in its own right. In the quark-hadron duality picture, the response averaged over resonances should equal that at higher Q^2, once target mass corrections and leading-log effects are taken into account [5, 6, 7, 8]. Because of the much different isospin structure and different couplings, the weak current will couple to individual resonances differently than the electromagnetic current, which can help in identifying new or poorly established resonances. We already have an indication that duality in the weak neutral current will work at the 20% to 30% level in a leading order valance picture of the vector hadronic current, as discussed in more detail below. What is of interest is to study the deviations due to the different mixture of resonances, their isospin structure, and their axial form factors. Since no measurements exist at present, it is not impossible that surprises await, and deviations from the leading order picture could be even larger than 30%.

A better understanding of the weak interaction at low Q^2 (1 to 2 GeV^2) is of great importance in understanding low energy neutrino interactions, which in turn are needed to determine neutrino masses and couplings through neutrino oscillation experiments ([9]). Since it is very difficult at present to produce mono-chromatic neutrino beams, or to measure their flux accurately, experimentalists generally assume quark-hadron duality for the weak current to predict total cross sections. The present proposal will test this crucial assumption for the first time. The mono-chromatic electron beam and good resolution spectrometers allow the kinematics to be very well determined, unlike in weak charged current experiments with neutrino beams.

Finally, PV inelastic scattering at low Q^2 should be measured "because it is there". JLab with 6 GeV is optimally poised to probe the kinematic range $M < W < 2.2$ GeV and $Q^2 < 1$ GeV^2 with high counting rates needed for PV experiments. PV experiments to date have focused on the more difficult exclusive measurements, which in the case of *ep* elastic scattering have an order of magnitude smaller asymmetry than inelastic scattering (for fixed Q^2). As illustrated in some of the examples above, inelastic electron scattering is connected to many experimental observables (either directly or through backgrounds), and provides a new tool to probe fundamental nucleon structure.

All of these observations suggest that it is long overdue to measure the PV asymmetry A_p and A_d in inelastic electron scattering at low Q^2. JLab is the only laboratory with sufficient beam energy and intensity to make these measurements in a meaningful way.

2 Physics

2.1 Parity Violating Asymmetry

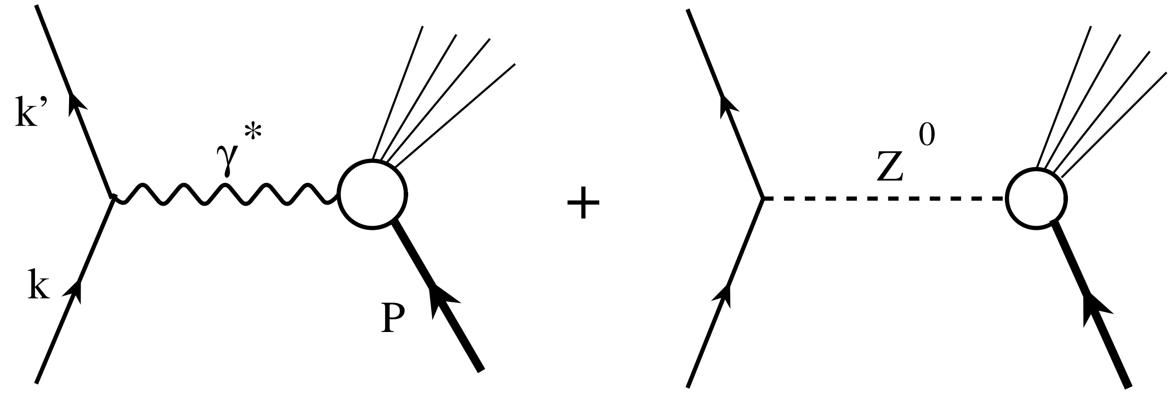

Figure 1: First order Feynman diagrams for lepton-nucleon scattering in the presence of a weak neutral current.

Fig. 1 shows the lowest-order Feynman diagrams for inelastic lepton-nucleon scattering for electromagnetic and weak interactions. Electrons can scatter off of protons by exchanging either a virtual photon, γ^*, or a Z^0 . Therefore the cross section for lepton-nucleon scattering can be written as,

$$d\sigma = d\sigma_\gamma + d\sigma_{weak} + d\sigma_I, \tag{1}$$

where $d\sigma_\gamma$ is the electromagnetic, $d\sigma_{weak}$ is the weak and $d\sigma_I$ is the interference contributions to the total cross section. For low-energy small-momentum-transfer lepton-nucleon scattering, the weak cross section is much smaller than the electromagnetic cross section, so the former can be safely neglected. However, the electromagnetic part is parity conserving, so the cross section is the same for right and left handed electrons, while the neutral current amplitude contains a parity violating term. Consequently the weak neutral current can be measured using the parity-violating asymmetry in the inclusive cross sections for electrons polarized parallel (R) and anti-parallel (L) to their momentum. The PV asymmetry is given by

$$A_{RL} = \frac{d\sigma_R - d\sigma_L}{d\sigma_R + d\sigma_L}. \tag{2}$$

Here $d\sigma_R$ and $d\sigma_L$ are the cross sections for scattering right and left handed electrons off an unpolarized target.

2.2 Resonance Region Asymmetry

In the nucleon resonance region, it is possible to describe A_{RL} in terms of response functions to specific final states, combined with a non-resonant background. In the one gauge boson (γ or Z^0) exchange approximation the asymmetry for scattering to discrete states can be written as [10], [11],

$$A_{RL}^{Res} = A_0 \frac{v_L R_{AV}^L(q,\omega) + v_T R_{AV}^T(q,\omega) + v_{T'} R_{VA}^{T'}(q,\omega)}{v_L R^L(q,\omega) + v_T R^T(q,\omega)}, \tag{3}$$

where L and T stand for longitudinal and transverse and $v_{L,T}$'s are lepton kinematic factors. The term $A_0 \approx 6.5 \times 10^{-4}$ [10] and the subscripts AV and VA denote axial-vector leptonic and vector hadronic currents and vector leptonic and axial-vector hadronic currents. The parity violating responses $R_{AV}^{L,T}$ can be decomposed in terms of their isospin content [10],

$$R_{AV}^{L,T} = \beta^{I=0} R_{L,T}(I=0) + \beta^{I=1} R_{L,T}^N(I=1), \tag{4}$$

$$\beta^{I=0} = -2\sin^2\theta_W, \qquad \beta^{I=1} = (1 - 2\sin^2\theta_W), \tag{5}$$

and I is the isospin quantum number. In the case of $N(1520)$, which is an isospin $\frac{1}{2}$ state, both terms in equation (5) contribute to the asymmetry. If one makes the approximation $\sin^2(\theta_w) = 0.25$ (so that the vector leptonic current, which multiplies the axial hadronic current, is zero), then in the limit of pure magnetic or electric scattering, and assuming isospin symmetry and negligible small strange and charm form factors, the proton asymmetry can be written as:

$$A_{RL}^{Res,p} = -0.9 \times 10^{-4} Q^2 \frac{\sigma_n}{\sigma_p}, \tag{6}$$

a remarkably simple equation. For the deuteron, the result becomes insensitive to nuclear structure with these approximations, and the simple prediction is simply:

$$A_{RL}^{Res,d} = -0.9 \times 10^{-4} Q^2. \tag{7}$$

Although the formalism for this was worked out long ago [17], to the best of our knowledge the details have so far only been worked out for the case of elastic scattering [12] and the $N \to \Delta(1232)$ transition [13], although there is an ongoing effort to understand the higher W region [10], in particular the influence of meson exchange currents. An approximate model for the $S_{11}(1530)$ resonance was very recently presented in the Ph.D. thesis of Sacco [14].

A detailed prediction of the $N \to \Delta(1232)$ proton asymmetry is given by [13] $A_p^\Delta = -(1.04 + 0.27F(Q^2, E, E', \theta_e) \times 10^{-4} Q^2$ where $F(Q^2, E, E', \theta_e)$ contains the information on weak form transition form factors, and is expected to be of order unity at for $Q^2 < 1$ GeV^2, decreasing to zero at very large E (or small $Q^2/2ME$) [12]. In the moderate Q^2 and energy of this proposal, this detailed prediction is within 20% of the simple model given by Eq. 6, since $\sigma_n/\sigma_p = 1$ for the isovector $\Delta(1232)$ resonance.

2.3 Deep-Inelastic Asymmetry

In the Standard Model and assuming quark degrees of freedom, the asymmetry arises from the interference between photon and Z exchange diagrams, and is given by [12]

$$A = \frac{\sigma_R - \sigma_L}{\sigma_R + \sigma_L} = -\frac{2Q^2}{M_Z^2} \frac{\sum f_i(x)(Q_i^\gamma/e)[g_A^e g_V^i + Y g_V^e g_A^i]}{\sum f_i(x)(Q_i^\gamma)^2}, \tag{8}$$

where $f_i(x)$ are the quark distribution functions for a quark of type i, the g's are the electroweak axial and vector charges, $Q^2 = -q^2$ is the four-momentum transfer squared ($Q^2 > 0$ for our kinematics), M_Z is the mass of the Z boson, and

$$Y = \frac{1-(1-y)^2}{1+(1-y)^2 - y^2 R/(1+R)} \tag{9}$$

where $y = \nu/E$, $\nu = E - E'$ is the energy lost by an incident electron of energy E scattering to an electron of energy E', and the factor $R = \sigma_L/\sigma_T$ takes into account [15] the longitudinal contributions to both Z and photon exchange. Performing the sums and re-writing M_Z in terms of the α and G_F coupling constants, for a proton target we obtain

$$A_p = \frac{3G_F Q^2}{\pi\alpha 2\sqrt{2}} \frac{2C_{1u}[u(x)+c(x)] - C_{1d}[d(x)+s(x)] + Y[2C_{2u}u_v(x) - C_{2d}d_v(x)]}{4u(x)+d(x)+s(x)+4c(x)}. \tag{10}$$

where the products of weak charges in the Standard Model at tree level are given by:

$$\begin{aligned} C_{1u} &= g_A^e g_V^u \\ C_{1d} &= g_A^e g_V^d \\ C_{2u} &= g_V^e g_A^u \\ C_{2d} &= g_V^e g_A^d. \end{aligned} \tag{11}$$

When Standard Model electroweak radiative corrections are included the C_{ij} become [16]

$$\begin{aligned} C_{1u} &= \rho'(-\frac{1}{2} + \frac{4}{3}\kappa' \sin^2(\theta_w)) + \lambda_{1u} \approx -0.1886 \\ C_{1d} &= \rho'(\frac{1}{2} - \frac{2}{3}\kappa' \sin^2(\theta_w)) + \lambda_{1d} \approx 0.3414 \\ C_{2u} &= \rho(-\frac{1}{2} + 2\kappa \sin^2(\theta_w)) + \lambda_{2u} \approx -0.0359 \\ C_{2d} &= \rho(\frac{1}{2} - 2\kappa \sin^2(\theta_w)) + \lambda_{2d} \approx 0.0265. \end{aligned} \tag{12}$$

In the limit of no electroweak radiative correction $\rho = \rho' = \kappa = \kappa' = 1$ and $\lambda_{1u} = \lambda_{1d} = \lambda_{2u} = \lambda_{2d} = 0$.

We have assumed that the $u(x)$, $d(x)$, $s(x)$, and $c(x)$ quark parton distribution functions (PDFs) of the proton can be described in terms of valence (v) and sea (s) contributions as

$$\begin{aligned} u(x) &= u_v(x) + u_s(x) + \bar{u}_s(x) \\ d(x) &= d_v(x) + d_s(x) + \bar{d}_s(x) \\ s(x) &= s_s(x) + \bar{s}_s(x) \\ c(x) &= c_s(x) + \bar{c}_s(x) \end{aligned} \tag{13}$$

The quark distribution functions depend mainly on the Bjorken scaling variable $x = Q^2/2M\nu$ (where M is the nucleon mass), but also evolve slowly with Q^2 due to QCD and finite mass corrections. While not shown explicitly, all quantities involving PDFs are functions of both x and Q^2.

In the valence region, A_p is numerically approximated using Eq. 12 and Eq. 10 by

$$A_p = -10^{-4}\ Q^2\ \frac{[0.51 + 0.45r(x) + 0.10Y(1 + r(x))]}{[1 + 0.25r(x)]}, \tag{14}$$

where we have ignored the strange and charm quark contributions, $r(x) = d(x)/u(x) \approx 1-0.75x$, and Q^2 is in units of GeV^2. Using isospin symmetry and with the approximation $\sin^2(\theta_w) = 0.25$, and ignoring strange and charm quark contributions, this can be written as

$$A_p = -0.9 \times 10^{-4}\ Q^2\ \frac{2(1 + \sigma_n/\sigma_p)}{5}. \tag{15}$$

The full equation for the deuteron asymmetry is given by

$$A_d = -10^{-4}\ Q^2\ \frac{[0.78 + 0.41R_c(x) + 0.37R_s(x) + 0.10YR_v(x)]}{[1 + 0.2R_s(x) + 0.8R_c(x)]}, \tag{16}$$

which when simplified in the valence region using $\sin^2(\theta_w) = 0.25$, can be written

$$A_d = -0.7 \times 10^{-4}\ Q^2, \tag{17}$$

which is about 20% less than the simplified transition form factor model.

2.4 Duality

Quark-hadron duality was first observed by Bloom and Gilman in 1970 [6]. It postulates that physical quantities calculated in the hadronic description give the same results as if they were calculated using the partonic description if a proper scaling variable that connects the two kinematic regions is used. In QCD, De Rujula, Georgi and Politzer [5] have shown that duality can be understood from an operator product expansion of moments of structure functions, which allows one to separate the short and long distance contributions to the moments of structure functions. The leading terms in the OPE correspond to scattering from free quarks, which are responsible for scaling, while higher terms take interactions between quarks and gluons (higher-twists) into account. In the resonance region if the higher-twists are significant then the moments of structure functions cannot be much different than the corresponding scaling value, which is given by the moments of the leading-twist term. Therefore, if a structure function rises above the scaling value it has to fall in the neighboring region (or oscillate around the scaling function) in order to compensate for the increase or decrease in the moments above the scaling value. This explains why resonances average to a smooth scaling curve. This behavior observed over restricted regions in W for each resonance is known as local duality. So far duality has been seen to work for unpolarized structure functions for the electromagnetic tensor, W_1^{EM} and W_2^{EM}, to Q^2 as low as 0.6 GeV^2. Fig 2 shows the structure function νW_2^{EM} as a function of the Nachtmann scaling variable, $\xi = 2x/[1+\sqrt{1+4x^2M_N^2/Q^2}]$, for different Q^2 values. The data clearly demonstrate that duality works remarkably well to rather low values of Q^2.

In terms of structure functions, to lowest order in the weak and electromagnetic currents, A_{RL} can be written as,

$$A_{RL} = \frac{Q^2}{Q^2+M_Z^2}\frac{g_A\left(2W_1Q^2+W_2(4EE'-Q^2)\right)-g_vW_3Q^2(E+E')/M}{2W_1^{EM}Q^2+W_2^{EM}(4EE'-Q^2)}, \tag{18}$$

where $W_{1,2,3}$ are structure functions for the interference tensor of the electromagnetic and weak neutral hadron currents, g_v and g_A are the vector and axial-vector coupling constants at the lepton-Z^0 vertex and E and E' are the energies of the incoming and outgoing electron. The denominator of the asymmetry A_{RL} depends only on W_1^{EM} and W_2^{EM}. Both these structure functions are very well measured and understood at the Q^2 values of this experiment and can be determined using a model. Although it is not possible to separate the structure functions for the interference tensor, A_{RL} can be used to test duality for a linear combination of W_1, W_2 and W_3 (numerator of equation (18)). Duality has never been tested for these structure functions to the date. As pointed out in the previous section depending on the isospin of the final excited state the interference cross section is expected to show a resonance structure.

Fig. 2.4 shows the expected asymmetry for the proton calculated with the simplified model of Eq. 6 and the σ_n/σ_p model of Keppel [18], at the two average Q^2 values of this proposal. Also shown is the DIS prediction, evaluated at the corresponding values of ξ, and a standard set of PDFs for $d(x)/u(x)$ to evaluate σ_n/σ_p. It can be seen that in this approximate model, duality appears to roughly work at both the local and global level. Essentially, the leading order criteria for duality to work can be written as

$$(\sigma_n/\sigma_p)^{res} = \frac{2}{5}\left(1+(\sigma_n/\sigma_p)^{DIS}\right) \tag{19}$$

The two different dependencies on σ_n/σ_p come from the fact that in the resonant case, the current is expressed through the square of the sum over parton charges, while in the DIS limit, it is the sum of the squares which gives the current. As pointed out by Close and Isgur [19], the cross terms can cancel on average when opposite parity states are mixed. In Fig. 2.4 it can be seen that the average of the $\Delta(1232)$ and the elastic peak

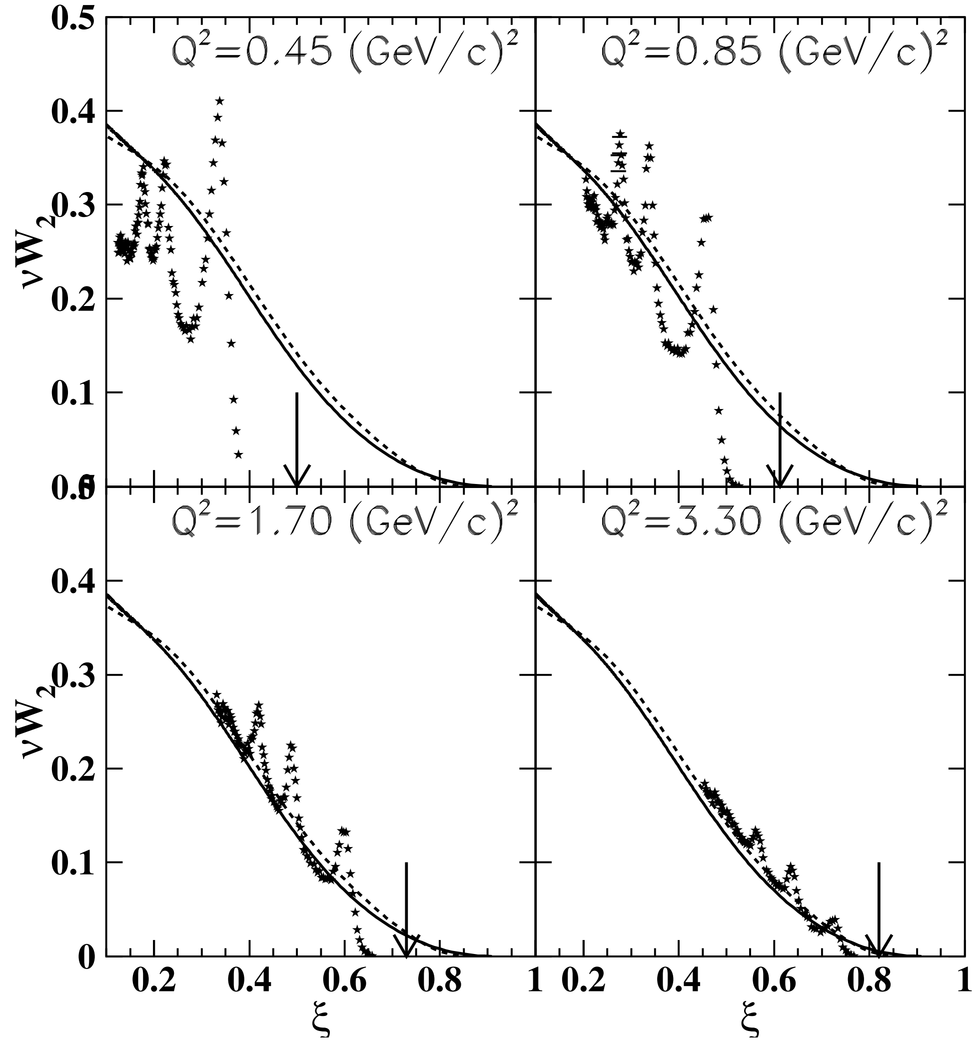

Figure 2: The spin independent structure function νW_2^{EM} plotted as a function of ξ for hydrogen at different Q^2 values [7]. The solid and dashed lines are a fit to deep inelastic structure function data at $Q^2 = 10$ (GeV/c^2) and $Q^2 = 5$ (GeV/c^2) respectively.

region tend to equal the DIS curve, and that at higher masses there are many resonances whose sum appears to oscillate around the DIS limit. We note that Eq. 19 is satisfied if on average $\sigma_n/\sigma_p = 2/3$, which is not a bad approximate of actuality.

In the case of the deuteron, the simplified formulas Eq. 7 and Eq. 17 differ by 20% at all kinematics, since both equations predict constant values.

Only with experimental data (which will include the effects of the axial current, strange form factors and higher twist contributions) will we be able to tell if duality works in actuality, and to what accuracy it works.

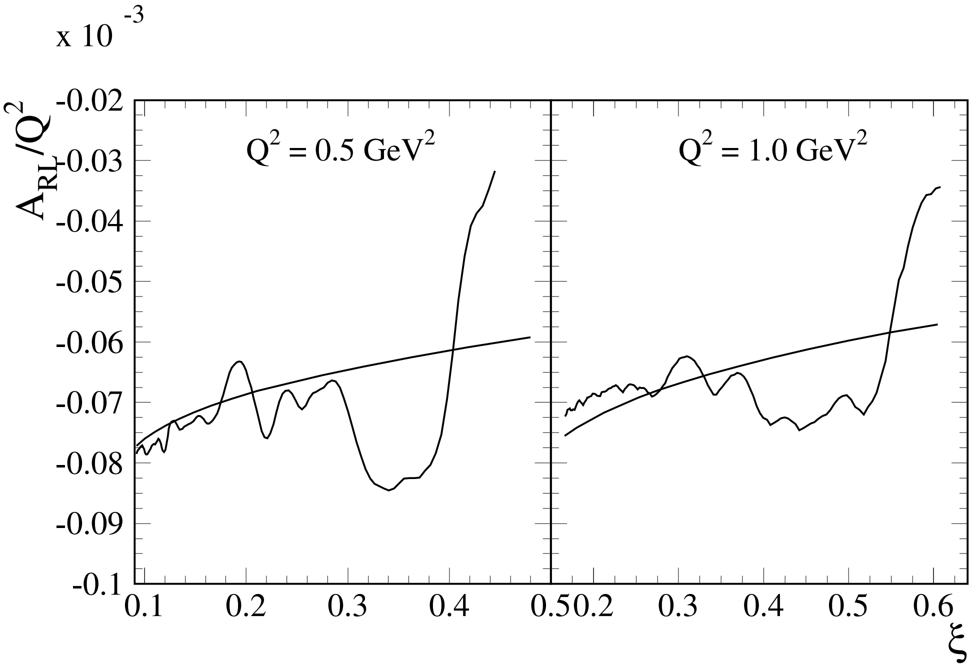

Figure 3: The oscillating curves are the simplified resonance region prediction for $A_p(W, Q^2$ in the limit $\sin^2(\theta_w) = 1/4$ from Eq. protect6 using the fit of Keppel [18] for σ_n/σ_p. The smooth curves are the DIS prediction from Eq. 14.

3 Experiment

The primary goal of the experiment is to measure A_p and A_d in and slightly beyond the traditional nucleon resonance region ($M < W < 2.2$ GeV) at moderate Q^2. The choice of hydrogen and deuterium as the targets is dictated by the desire to observe possible resonance structure, without the large blurring effects of Fermi motion and shadowing in heavier nuclei, and to test duality using the weak neutral current with two isospin combinations, for which the predictions are quite different, as was discussed above. Measurements with both hydrogen and deuterium have a further advantage, in that the ratio of asymmetries is almost free of experimental systematic errors, allowing a very precise comparison with theory.

The range of Q^2 to be explored is limited to about 0.4 GeV^2 on the low end due to increasingly large elastic radiative tails at low Q^2 (which dilute the measured asymmetry), and by the smallest practical scattering angle for a large solid angle spectrometer. The range of Q^2 on the high end is limited to about 1 GeV^2 by the maximum beam energy of 6 GeV and the rapidly decreasing cross sections with increasing Q^2. The range of $0.4 < Q^2 < 1$ is well matched to that where the onset of duality is seen to occur in the spin-averaged proton response functions, as well as the spin-dependent structure function g_1 [20].

The experimental asymmetry is diluted by the beam polarization P_e, so that

$$A_{exp} = \frac{N_+ - N_-}{N_+ + N_-} = P_e A,$$

where N_+ and N_- are the number of scattered electrons detected from + and − beam helicities respectively. The statistical uncertainty is given by

$$\delta A = \frac{1}{P_e\sqrt{N_+ + N_-}}.$$

For Q^2 in the 20 GeV^2 range, on the order of 5×10^9 electrons must be detected to achieve a 1% uncertainty in the physics asymmetry.

For $Q^2 = 1$ GeV^2, typical asymmetries are of order 100 ppm, large compared to the typically few ppm asymmetries of HAPPEX or G0 experiments at JLab, and comparable to the raw asymmetries measured in Hall B with polarized electrons incident on polarized deuterons in ND3. This makes the requirements on beam systematics for this proposal (charge and position asymmetries and jitter, leakage from other Halls, etc.) considerably more relaxed than in previous PV experiments at JLab.

3.1 Optimization of kinematics

Several considerations enter into the optimization of beam energy and spectrometer angle. The beam energy E must be at least 3 GeV to span the full resonance region. In practice, a higher beam energy of 4 GeV is needed to avoid large radiative tails at high W. For a given choice of Q^2, the figure of merit (FOM) improves approximately linearly with E, due to the larger cross section at the correspondingly smaller angles. Therefore the maximum available beam energy of 5.5 to 6 GeV is optimum.

For $Q^2 = 1$ GeV^2, the corresponding scattering angle is 11 degrees, which happens to match the minimum HMS spectrometer angle in Hall C. To extend the Q^2 range down to 0.4 GeV^2, a lower beam energy of about 4 GeV is optimal, if the minimum scattering angle is fixed at 11 degrees.

3.2 Choice of Spectrometer

In Hall A, the HRS spectrometers could be used at 6 degrees with the septum magnets, but the maximum momenta of 3.2 and 4.0 GeV are too low to match the scattered electron momenta with a 6 GeV beam. The SOS spectrometer in Hall C is limited to 1.7 GeV. The HMS spectrometer in Hall C covers the full momentum range needed (up to 5.5 GeV) and can go down to 11 degrees, so is well-suited to measurements near $Q^2 = 1$ GeV^2. A custom spectrometer centered at 9 degrees could also be used for parasitic running with the GEP-III and GEP-2γ experiments: this is discussed in Appendix A. Any differences from the HMS option presented in the main section of the proposal are spelled out in this Appendix.

4 Target

We would like to use 25 cm long cryogenic loops, rather than the standard Hall C 15 cm loops, to obtain the highest possible luminosity. We assume that at full beam energy the highest reliable beam current is about 80 μA. With this current, the existing cooling capacity is fully capable of supporting 25 cm long cells. At 11 degrees, the HMS acceptance is only reduced by a few percent in going from 15 cm to 25 cm cell lengths. Of Hall C experiments may benefit from the longer cells as well.

5 Detectors

The basic detector concept is that of a segmented electromagnetic shower detector to optimize the signal-to-background for electrons in a single detector. This technique was successfully pioneered by the original SLAC DIS-parity experiment [1]. The lead glass blocks in the HMS spectrometer are well-suited to this purpose. The blocks are 10 cm tall by 10 cm deep and 70 wide. There are four layers in the electron direction, and 13 blocks vertically, corresponding to different average values of W. The front two layers have PMTs on each end, while the back two layers only have PMTs on one end. We plan to measure the asymmetry for each PMT, as described in more detail in the electronics section below. The primary results will be from the second layer, where the average electron signal is 15 to 20 times larger than the average pion signal (as determined from actual data with HMS central momentum of 3.5 GeV). We plan to add 10 r.l. (2 inches) of lead between the third and fourth layers, so that the electron signal in the fourth layer is essentially zero, while the pion signal will be only slightly changed. The fourth layer will therefore measure the pion asymmetry (as well as that of any soft isotropic background). We will then correct each layer of the front three layers for the dilution and asymmetry of the pions. A valuable systematic check will be provided by the consistency of the results from each of the front layers. Since the π/e ratio is < 1 for all the kinematics of this proposal, the corrections are relatively small (0.1% at low W to 10% at high W) for the second layer of lead glass, we don't need to perform event-by-event pion rejection (for example using a coincidence with the gas Cherenkov counter), which would greatly complicate the electronics for the very high particle rates of this experiment.

The statistical fluctuations on the signals integrated over each helicity bucket will be increased by less than 10% above $1/\sqrt{N}$ by the fluctuations in the amount of Cherenkov light generated per electron a shower maximum, and by the light collection efficiency, which varies by about $\pm 15\%$ over the length of the lead glass blocks. The light output will be energy-weighted, which is useful in partially compensating for the linear Q^2 variation of the asymmetry.

The lead glass blocks will be read out by the existing PMTs with tube bases that may be modified if needed for good linearity at the expected very high event rates (see Table 1). Tests will be made to ensure better than 2% linearity in the operating range used.

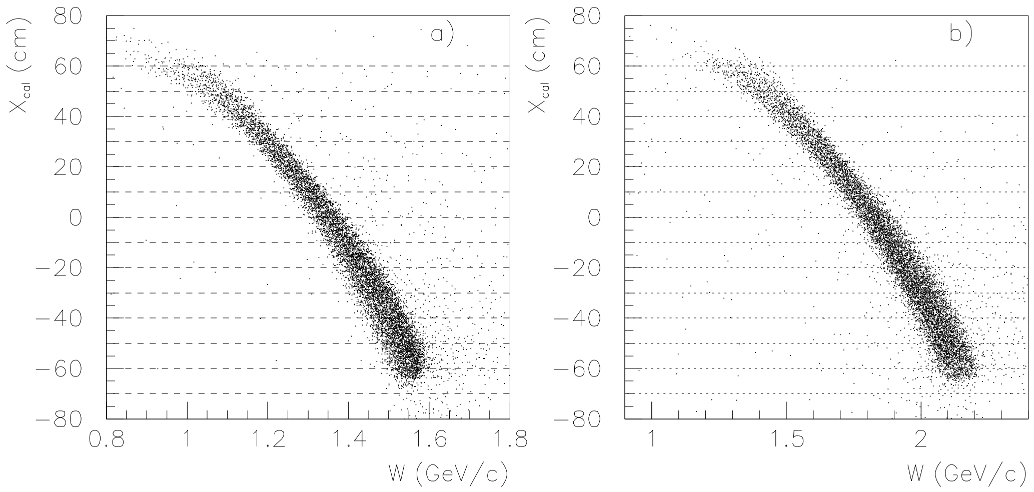

Figure 4: Missing mass W as a function of detector position for $E = 6$ GeV and: a) the high momentum HMS setting; b) the low momentum HMS setting. The horizontal bars indicate the 10 cm spacing of the lead glass blocks.

6 Electronics

Each PMT of each detector, a total of about 78 channels, will be read out for each helicity state at 30 Hz by both integrating electronics. The integrating method will give us a reliable, proven method of readout which is free from dead-time corrections.

We plan to use the HAPPEX DAQ or a similar style DAQ. Members of HAPPEX have agreed to collaborate on the DAQ setup. The integrating DAQ may consist of either the custom 16-bit integrating ADCs, or since the asymmetries are rather large ($>$ 30 ppm) we could alternatively integrate with a simple setup of voltage-to-frequency converters plus scalers which other experiments have used at JLab, including non-parity experiments like g_2^n in Hall A. The integrating DAQ will also record the beam-line monitors in each helicity pulse, i.e. the charge and the positions at the target and in a dispersive region (sensitive to the energy). This will allow us to evaluate systematic errors in the beam parameters as is customary for parity experiments. We note that the demands of this proposal on beam systematics are less stringent than for HAPPEX or G0.

We also plan to instrument at least one of the detectors in each layer with VME Flash ADC modules. These will be used for detailed studies of the pulse height distributions and correlations between the four layers.

Particles that pass near the boundaries of the lead glass blocks will generate correlations in the asymmetries of adjacent blocks. This will be accounted for using a detailed simulation of the lead glass response, as was done in previous PV experiments such as SLAC E158 [4]. The simulation will be calibrated using data at lower luminosity and the

Table 1: Kinematic variables, pion/electron ratio, expected asymmetry, and expected relative asymmetry error for bins approximately centered on groups of three lead glass detectors, for a beam energy of 6 GeV, and 60 hours (30 hours) for each of two HMS central momentum settings for LH2 (LD2).

W (GeV)	x	Q^2 (GeV^2)	Y	E' (GeV)	π/e	rate (kHz)	A (ppm)	dA/A (%)
				LH2				
2.16	0.17	0.78	0.50	3.55	0.41	236.9	57.4	9.07
2.05	0.20	0.84	0.44	3.79	0.21	269.4	59.7	8.17
1.92	0.24	0.89	0.39	4.03	0.11	281.1	61.8	7.73
1.79	0.29	0.94	0.33	4.26	0.06	292.7	63.4	7.38
1.64	0.35	0.99	0.28	4.50	0.03	311.3	64.6	7.03
1.49	0.44	1.04	0.23	4.74	0.01	344.0	65.0	6.64
1.31	0.57	1.10	0.19	4.97	0.01	219.7	64.4	8.38
1.10	0.77	1.15	0.14	5.21	0.00	223.8	62.6	8.20
				LD2				
2.16	0.17	0.78	0.50	3.55	0.45	470.4	74.8	6.98
2.05	0.20	0.84	0.44	3.79	0.25	503.8	76.8	6.57
1.92	0.24	0.89	0.39	4.03	0.13	535.6	78.5	6.23
1.79	0.29	0.94	0.33	4.26	0.07	559.2	80.0	5.98
1.64	0.35	0.99	0.28	4.50	0.03	566.8	81.5	5.83
1.49	0.44	1.04	0.23	4.74	0.01	567.9	83.4	5.70
1.31	0.57	1.10	0.19	4.97	0.00	626.4	85.8	5.27
1.10	0.77	1.15	0.14	5.21	0.00	537.0	89.1	5.49

full package of HMS detectors (gas Cherenkov, scintillator paddles, and drift chambers).

As discussed in more detail below, the consistency of the corrected asymmetries from each of the three front layers will provide a valuable check on systematics. Another check will come from the consistency of the results from the dual PMTs (one at each end) for the front two layers. Finally, we will also instrument the gas Cherenkov counter in flux integration mode. Since the threshold is set so that only electrons make a Cherenkov signal, and pions only make 0.1% as much light on average through knock-on electrons, the Cherenkov asymmetry will be a valuable systematic check on the average lead glass asymmetry. This technique was also used in the SLAC experiment [1].

The gains for the lead glass PMTs will be adjusted to give good linearity. Because the electron particle flux is only about a factor of five higher than regular HMS running at forward angles (for which good linearity has already been observed), the gain adjustment will likely not need to be large. We will perform a series of test measurements to determine if the tube bases need to be modified for better linearity at our roughly < 600 kHz rates per detector. We will be able to monitor the PMT gains using the measured luminosity, and also a laser pulse system, if needed.

Table 2: Expected results for 30 hours at each of two HMS settings for LD2 and a beam energy of 4 GeV.

W (GeV)	x	Q^2 (GeV^2)	Y	E' (GeV)	π/e	rate (kHz)	A (ppm)	dA/A (%)
1.94	0.11	0.34	0.52	2.29	0.86	836.4	35.2	11.11
1.85	0.12	0.36	0.46	2.46	0.51	936.0	36.4	10.16
1.76	0.15	0.38	0.41	2.62	0.29	1053.5	37.4	9.33
1.66	0.18	0.41	0.35	2.78	0.16	1188.0	38.1	8.63
1.56	0.22	0.43	0.30	2.95	0.09	1328.5	38.5	8.06
1.45	0.27	0.46	0.25	3.11	0.04	1443.7	38.8	7.68
1.33	0.35	0.48	0.20	3.27	0.02	1528.6	39.1	7.41
1.20	0.48	0.50	0.15	3.43	0.00	2239.0	39.6	6.04

7 Expected Results

7.1 Kinematic Coverage

The kinematic coverage in W, Q^2, x, and Y is shown in Table 1 for the 6 GeV beam energy, and in Table 2 for 4 GeV beam energy. At both energies, the full resonance region $M < W < 2.2$ GeV is covered, with an average Q^2 of 1 GeV^2 for $E = 6$ GeV, and 0.4 GeV^2 for $E = 4$ GeV. Since the HMS momentum acceptance is approximately $\pm 10\%$, two central momentum settings are needed at each beam energy, as can be seen from the E' values listed in the Tables.

7.2 Choice of Targets

We propose to use both LH2 and LD2 for the 6 GeV running near $Q^2 = 1$ GeV^2. While we would like to study both targets at lower Q^2, in the interest of saving valuable beam time we choose to use only LD2 for the lower Q^2 running, because the errors on LD2 are about 40% smaller for LD2 than for LH2 for a given running time, and the ratio of asymmetries is not expected to be strongly Q^2 dependent.

7.3 Statistical Errors

The expected statistical errors are listed in Tables 1 and 2. The W bins approximately correspond to 3 adjacent lead glass blocks, and are spaced to roughly correspond to the experimental resolution in W. Resonant structure on the scale of 10% will be clearly visible with these data: this is small compared to the 30% to 50% resonant fluctuations of the unpolarized structure functions around the smooth duality curve. For tests of local duality, we can divide the resonance region into four regions in W, and in each region will be able to test local duality at the level of about 4%. This seems quite adequate

Table 3: Estimated experimental systematic errors on dA_p/A_p and dA_d/A_d.

source	$\delta A/A$
Beam Polarization	0.012
Kinematic determination of Q^2	0.010
Detector and Electronics Linearity	0.005
Electromagnetic radiative corrections	0.005
Beam asymmetries	0.005
Pion contamination	0.005
Pair symmetric background	0.002
Target purity, density fluctuations	0.002
Total	0.02

for a pioneering measurement. The statistical error for a test of global duality (averaged over the entire resonance region) will be at the level of 2%, which is well-matched to the anticipated systematic error (see below), The error on the ratio of averaged proton and deuteron asymmetries will be about 3%, with a much smaller systematic error (since most of the systematic error cancel in the ratio).

The expected systematic errors are tabulated in Table 3, and discussed in the following sub-sections.

7.4 Beam Polarization

The beam polarization will be measured using the standard Hall C Møller polarimeter. The expected error averaged over each beam energy is about 1.2%, which will be a common systematic error to all results. To achieve this error, we would like to make at about eight polarization measurements (which take about an hour each) over the course of the run. We also hope to implement a scheme to measure polarization at full beam current (for a subset of beam pulses), rather than at the present limit of 2 μA.

7.5 Kinematic determination of Q^2

Since the raw asymmetry has a linear dependence on Q^2, but a small dependence on other kinematic variables such as W or x, the largest systematic error in the physics asymmetry determination arises from the knowledge of the average Q^2 of the events seen in each detector, weighted by detector response. The average Q^2 will be determined from a detailed model of the spectrometer apertures and magnetic fields. Since the HMS spectrometer is very well understood from previous experiments (which have measured absolute cross sections at the 1% level), our preliminary studies indicate that we will be able to determine the average effective Q^2 to better than 1%.

The uncertainty in beam energy E is less than 0.02%, which contributes a negligible uncertainty to $Q^2 = 4EE' \sin^2(\theta/2)$. The HMS central momentum is known to $< 0.1\%$, and the central angle to better than 1 mr. These generate an uncertainty in the central Q^2 value of about 0.8%.

7.6 Electronics and detector non-linearity and pedestal shifts

Parasitic studies of the PMT response will be made to ensure that non-linearity in the tube base and integrating electronics results in less than 0.5% false asymmetry. Careful attention will be paid to the problem of a helicity-dependence caused by room background. This will be measured by an extra lead glass detectors placed outside the acceptance of the spectrometer. A PMT not connected to any detector will also be placed outside the acceptance to measure the effect of backgrounds interacting in the photocathodes.

7.7 Electromagnetic Radiative Corrections

Electromagnetic radiative corrections arise from the emission of photons by either the incident or scattered electron, either in the field of the nucleus (internal corrections), or in the field of another nucleus (external corrections). The ratio R_U of un-radiated to radiated spin-averaged cross sections is shown in Fig. 5 for the two beam energies. At high W (low electron momentum P), the radiated cross section is larger than the Born cross section, while the reverse is true at high W. In the kinematics of this proposal, R_U is mainly determined by the (x, Q^2) dependence of the spin-averaged structure function F_2. Of particular relevance is the ratio R_P of radiated to un-radiated *ed* parity-violating asymmetry. This ratio is close to unity for the kinematics of this proposal. The shape and magnitude of R_P is primarily determined by the probability for an electron to radiate a hard photon, and to a lesser extent by the (x, Q^2) dependence of F_2 and A_p. We have estimated the systematic error in A_p to be $< 1\%$ over most of the kinematics of this experiment by considering the uncertainty in the unpolarized cross section (using several fits to world data) and in A_p, which will be largely determined by an iterative fit to the data of this proposal (although the elastic contributions to A_p are already reasonably well known from previous experiments). Uncertainties in the target dimensions and various materials which act as radiators have much smaller effects. These calculations were performed in the peaking approximation of Mo and Tsai [21]. Calculations with the more exact formulas of Ref. [22] are planned.

7.8 Electroweak Radiative Corrections

Interpretation of the experimental results in terms of transition form factors (both axial and vector) requires the careful treatment of electroweak radiative corrections. In the case of the $\Delta(1232)$ resonance, these can be sizable, and increase in relative importance as $Q^2 \to 0$ [23]. We are not aware of calculations for higher mass resonances. For the interpretation of the data in terms of quark-hadron duality, and for simply searching

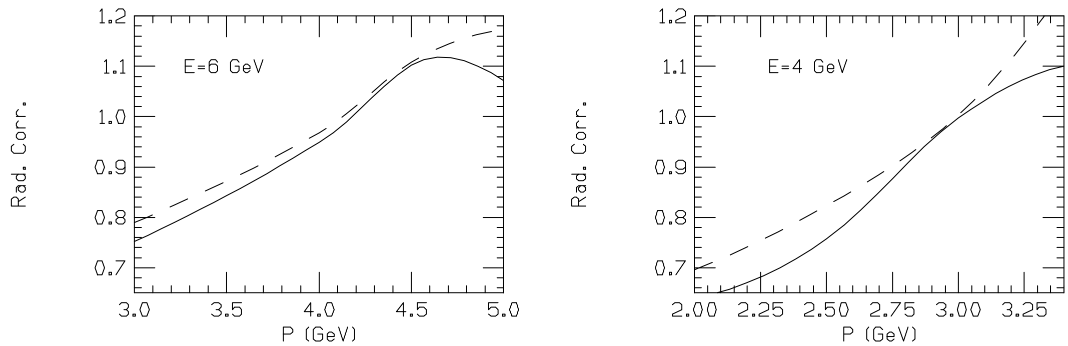

Figure 5: Radiative correction as a function of scattered electron momentum P for $E = 6$ GeV (left) and $E = 4$ GeV (right).

for resonance structure in A_p, it is not crucial to have a complete understanding of electroweak radiative corrections, so we haven't included an uncertainty in the systematic error table. However one should keep in mind their importance in the interpretation of the data in terms of specific transition form factors.

7.9 Beam Asymmetries

Since the raw asymmetry in this experiment is 50 to 1000 times larger than other JLab PV experiments, our requirements on beam position, angle, energy, and charge asymmetries are relatively modest, comparable to those of Hall B EG1. We are therefore confident that the sophisticated beam feedback system used in G0 is not needed, and we are not requesting it because it takes a considerable overhead in beam time to keep it calibrated. We will monitor all beam asymmetries on-line, and request improvements if they become unacceptably large.

We will periodically reverse the half-wave plate at the injector to help cancel any residual false asymmetries.

7.10 Pion Contamination

The predicted π/e ratios shown in Table 1 and 2 are based on a fit to pion photoproduction data [24], which has proven to be accurate to 30% or better in past experiments. The π/e ratio is strongly W-dependent, approaching 1 in the highest W bin. We will measure the π/e with a relative accuracy of better than 5% in a short counting mode run, and the pion asymmetry with a statistical accuracy of about 10%. The systematic error for the flux-integration electronics will be about 1% at the highest W, and about 0.5% on average, because the average pion signal in the front three layers of lead glass is less than 10% of the electron signal. A valuable systematic check will be obtained from the consistency of the extracted electron asymmetries from each of the three front layers.

The sign and magnitude of the pion asymmetry is of some physics interest in it's own right, especially as it may impact backgrounds in experiments such as E158 and

G0. It was seen to be small in the original SLAC experiment [1]. While we don't know of any calculations of the pion photoproduction asymmetry at our kinematics, the predicted asymmetry is of order 10^{-7} at energies below 0.55 GeV [25], and 1.3×10^{-6} for excitation of the $\Delta(1232)$ resonance [26]. These are both negligible compared to our expected electron asymmetry of about 1×10^{-4}.

7.11 Pair Symmetric Background

In addition to the electron scattering events of interest, electrons can originate from decays of vector and pseudo-scalar mesons, and wide angle pair production. To a very good approximation, these processes are pair-symmetric, and can be measured with better than 3% accuracy by reversing the polarity of the spectrometers. Based on simulations with PYTHIA [27],we expect the largest source of pair-symmetric events to be from decays of photoproduced π^0 mesons. The simulation is in reasonable agreement with data taken in Hall C over the past years. The highest predicted e^+/e^- ratio for this proposal is about 0.5% (at $W = 2.2$ GeV), and drops rapidly at lower W. The asymmetry is expected to be very small, and this will be verified by taking data for a few hours with reversed spectrometer polarity. The net relative uncertainty on A_p and A_d will be $< 0.2\%$.

7.12 Target Density Fluctuations

Target boiling effects have been shown to be very small for the 15 cm LH2 and LD2 targets in Hall C with currents up to 100 μA. Target density fluctuations introduced by local heating for our proposed 25 cm LH2 and LD2 targets with 80 μA are expected to be at 0.01% level of less, based on experience in E158, G0, and HAPPEX. Since our raw asymmetry error per detector per pulse pair is about 2%, this leads to a negligible increase in effective statistical fluctuations.

A small-angle luminosity monitor similar to that used in HAPPEX will be used to verify a null asymmetry and provide additional confidence that target density fluctuations and helicity-correlated beam asymmetries are small.

With a magnetic field at the target of < 10 Gauss, the proton polarization will be less than 0.001%, leading to a negligible double-spin asymmetry from the g_1 structure function.

Impurities in the liquid hydrogen are typically less than 0.1%, and are expected to cause a negligible effect on A_p since the asymmetry has only a weak dependence on atomic number A. The largest effect will be from the aluminum endcaps, for which the asymmetry is typically 20% larger than for the proton is the DIS limit. Since the endcaps contribute only a few percent of the count rate, this correction is small, and will be constrained by the deuteron A_d measurements, for which the asymmetry is almost the same as for aluminum. For the deuteron measurements, the biggest correction comes from the fraction of hydrogen. This will be measured to better than 0.2%, leading to a negligible systematic error on A_d.

8 Request

Our primary request is to perform this experiment with the HMS spectrometer as a dedicated experiment. If limitations on available beam time make this impossible, an alternate request is presented that could achieve most of the goals of the proposal in parasitic running with the two GEP experiments.

8.1 Primary Request

We request 10 days of production data and one day for checkout, beam polarization measurements, and configuration changes, as summarized in Table 4. We are flexible on the exact beam energies: the higher beam energy can be anything above 5.2 GeV, and the lower beam energy anything between 3.6 and 4.2 GeV. We request a modest electronics budget to instrument the PMTs of the HMS spectrometer with flux-integrating ADCs. Modified tube bases may be needed for good linearity at 600 kHz rates (to be determined by parasitic tests). A small investment will also be needed for the luminosity monitor. If the 25 cm targets are already in place for another experiment, the only change to the standard HMS configuration is the addition of lead between the third and forth lead glass layers.

8.2 Primary Request

We request 10 days of production data and one day for checkout, beam polarization measurements, and configuration changes, as summarized in Table 4. We are flexible on the exact beam energies: the higher beam energy can be anything above 5.2 GeV, and the lower beam energy anything between 3.6 and 4.2 GeV. We request a modest electronics budget to instrument the PMTs of the HMS spectrometer with flux-integrating ADCs. Modified tube bases may be needed for good linearity at 100 kHz rates (to be determined by parasitic tests). A small investment will also be needed for the luminosity monitor. If the 25 cm targets are already in place for another experiment, the only change to the standard HMS configuration is the addition of lead between the third and forth lead glass layers.

8.3 Alternative Request

Our alternative request is to run jointly with E04-108 and E04-019 (collectively: GEP-III+) for a total of 58 PAC days at energies of 2.2 to 6 GeV (with the bulk of the running, 38 days, at 6 GeV). We request an additional 1 PAC days for extra Møller beam polarization measurements and dummy target running (which will also benefit GEP-III+), and 1 PAC day of dedicated *ep* coincidence measurements between HMS and the Res-Parity spectrometer for calibrations. Therefore our total request is for 2 PAC days beyond GEP-III+. We request resources to install three existing magnets in Hall C and connect them to power and water. The magnet will need alignment and magnetic field measurements to check the model calculations. An existing slit system

Table 4: Beam time request using HMS spectrometer.

E	Target	P HMS	time
6 GeV	LH2	4.0 GeV	60 hours
6 GeV	LH2	4.8 GeV	60 hours
6 GeV	LD2	4.0 GeV	30 hours
6 GeV	LD2	4.8 GeV	30 hours
4 GeV	LD2	2.6 GeV	30 hours
4 GeV	LD2	3.1 GeV	30 hours
Checkout			8 hours
Pass Change			8 hours
Polarization			8 hours
E^+ Asymmetry			4 hours
Total			11 days

will be needed to define the solid angle for different running configurations. Existing lead glass detectors with PMTs will be used from the SOS spectrometer and from existing spares. The electronics and luminosity monitor are essentially the same as for the HMS option.

9 Physics Summary

The physics results will be the first ever measurements of the PV asymmetry in inelastic electron scattering from the proton in the resonance region beyond the $\Delta(1232)$. The precision will be sufficient to observe resonance structure at the 5% level, and to test local and global duality at the few percent level. The results will not only be interesting in their own right as a new way to probe the fundamental structure functions of the proton and neutron,but will be of great value in the growing world-wide program of neutrino studies. The new data may also provide insights into backgrounds in other PV experiments, and are needed as input to DIS-parity studies at higher Q^2 through radiative corrections.

10 Collaboration

The collaboration has many members with recent experimental experience in precision electron PV experiments (such as SLAC E158 and JLab HAPPEX), and we are confident that we will be able to control systematic errors at the few percent level. The collaboration includes the group that built and maintains the HMS/SOS lead glass detectors, which are key elements of this proposal. If the parasitic option takes place, the

Table 5: Optical model of the Res-Parity spectrometer. Offsets and horizontal angle θ_H are relative to a nominal 9° center line with respect to the beam axis. The length is the effective magnetic length, and the field is the average over the length. For the quadrupole, the field is at a radius of 35 cm.

Element	Length	B	Offset	θ_H
Drift	3.00 m	x	x	x
D1	0.70 m	19 kG	0.	43 mr
Drift	2.00 m	x	x	x
Q1	1.00 m	12.3 kG	20 cm	86 mr
Drift	0.70 m	x	x	x
D2	1.45 m	19 kG	35 cm	176 mr
Drift	6.2 m	x	x	x

collaboration includes members with extensive experience in spectrometer design and construction.

11 Appendix A: Parasitic Spectrometer Option

The two GEP-III+ experiments will run for 58 days with polarized electrons on unpolarized hydrogen. There is room on the SOS side of the beam for a custom spectrometer to perform most of this proposal in a parasitic mode. Since there are no spare super-conducting quadrupoles available to make such a spectrometer, the solid angle is necessarily smaller than those of the HMS or HRS spectrometers. However, this is offset by the relatively long running time of GEPIII+, which will run for a relatively long 58 PAC days with beam energies of 2 to 6 GeV, with the bulk of the running (38 days) at 6 GeV.

11.1 Spectrometer

The spectrometer for this option is a DQD design. The dispersion is in the scattering plane, so that physics scattering angle θ and electron momentum P are mixed in the horizontal plane, while the azimuthal angle ϕ is isolated in the vertical plane. This optics are optimized to focus particles at constant W onto distinct positions at the detector, so that the asymmetry can be measured as a function of W by flux integration of distinct detector elements.

Summaries of the optical model and magnet parameters are given in Tables 5 and 6. The first magnet is the splitter magnet (D1) from the HKS experiment. The is a C-type magnet which we will use with the return iron away from the beam line, allowing the opening to be placed close to the beam line. This acts like a septum magnet to allow electron scattering angles down to 7 degrees. Shims will be bolted to the pole

Table 6: Magnet apertures and approximate operational current and voltage.

Magnet	width	height	Current	Voltage
D1	25 cm	7.5 cm	1000 A	150 V
Q1	70 cm	14 cm	1000 A	100 V
D2	55 cm	25 cm	1000 A	250 V

face (using existing bolt holes) to provide a uniform field integral of 1.33 Tm with a minimum gap of 7.5 cm (the nominal gap is 15 cm, with a small field gradient due to the C-type construction). This is followed by the large Serayevo quadrupole (Q1) used in T20. This is a Panofsky-type quadrupole, with a large horizontal opening (± 35 cm) and a small horizontal opening (± 7 cm on the edges). This quadrupole is the main horizontal focusing element to allow events to be measured as a function of W at the detectors. This magnet has an extra weak dipole/sextupole coil winding which will be energized to it's maximum current of 150 A to provide a little extra dispersion and to rotate the focal plane ($B = 0.378 + 6.18x^2$ kG, where x is horizontal displacement in m). The final magnet is the 1.45 m effective length MIT dipole (D2, also known as Charybdis) that was used in T20 and the Madey *et al.* GEN experiment. This provides the bulk of the dispersion needed to separate different values of W at the detectors.

The spectrometer optics are illustrated in Fig. 6. In the horizontal plane, scattering angle and momentum are mixed to provide a focus in W. The focal plane is strongly titled, intersecting the detector plane for $W = 1.5$ GeV (the middle of the range to be studied). Adequate W separation is still provided for $1 < W < 2.2$ GeV. In the vertical plane, the particles are defocused by Q1. Since there is no physics in the out-of-plane angle, the detectors are only segmented in the horizontal direction. The solid angle of the spectrometer varies from 1.3 msr to 1.1 msr for $W = 1$ to 2.2 GeV. To obtain two distinct Q^2 ranges, we will use the slits two define two ranges of scattering angles. The solid angle in each setting is about 0.6 msr.

The layout of the spectrometer in Hall C is shown in Fig. 7. The magnets (just barely) clear the beam line planned for GEP-III+, and the magnets also fit within the angular range needed for the smallest angle planned for the Big-Cal calorimeter (here shown at 30 degrees).

The SOS power supplies will be used to power the magnets for the proposed spectrometer. These will all be running close to their maximum current of 1000 A. The two 160 V supplies will run D1 and Q1 (actual voltages needed are 150 A and 100 A respectively), while the 250 V supply will run the dipole. A smaller existing supply will run the sextupole coil of Q1, which needs 41 V and 150 A. Water cooling will be done as in in T20.

An existing movable slit system will be placed in front of D1 to define a range of horizontal scattering angles. We plan to run with two slit settings ($7 < \theta < 9$ degrees and $9 < \theta < 11$ degrees) two obtain two distinct average Q^2 values. The slits will also be used to study the acceptance as a function of scattering and out of plane angles.. The vertical acceptance will be defined by the collimator to minimize the effect of electrons striking the polarized iron in the magnet pole faces.

The average flight path for the spectrometer is about 15 m, which corresponds to 5% r.l. of air. This will cause radiative energy loss and multiple scattering at a moderate level, and will degrade the W resolution. While cost considerations preclude the option of a vacuum chamber, we may elect to put a helium chamber along the flight path.

The more conventional alternative of having the dispersion in the vertical direction was studied. The disadvantages are: small Q^2 range (assuming the angle must remain fixed during the experiment to facilitate construction); minimum angle larger (so cannot go to as low Q^2); detectors closer to the beam line (so more background); available magnets would have to be rotated from their conventional positions and at least one magnet would have to be tilted (requiring a custom support stand); the largest available quadrupole (Serayevo) is very wide if rotated by 90 degrees, limiting even more the smallest possible scattering angle.

11.2 Detectors and electronics

A front layer of 5 r.l. (one inch) of lead is used to create a large electromagnetic shower. Behind this there is a layer of lead glass blocks, each 10 cm wide,10 cm deep, and 70 cm tall, with the PMTs mounted on both the top and bottom of each block. Thirteen blocks placed side-by-side are needed to span the full W region of interest. These blocks will be taken from the SOS spectrometer and from the Hall C supply of spare counters. The W range spanned is approximately the same as for the two HMS settings combined. The resolution in W varies from 0.1 to 0.13 GeV (best at $W = 1.7$ GeV).

The DAQ and electronics are the same as for the HMS option.

11.3 Special Studies

We will check the magnetic optics by comparing the electron rate as a function of position with the simulation at each beam energy. The *ep* elastic peak is particularly useful in this regard, especially for $E = 4.8$ and 3.0 GeV, where it can be sharply focused onto the detectors. We plan to do special calibration runs with the HMS detecting the corresponding recoil protons at angles from 58 to 71 degrees and momenta from 0.5 to 1 GeV. Aside from calculate radiative effects, there should be one electron detected in the predicted lead glass block of the res-parity spectrometer for every proton detected in the HMS. For this studies, we will use about 0.5 days of dedicated beam time per primary beam energy (for a total of 1 day).

We will also do special runs to compare the detector rates as a function of the horizontal slit setting in front of D1, and also with/without a vertical aperture defining collimator. We will also study the rates as a function of quadrupole setting and compare them with our model.

With all of these studies, we are confident that we can determine the effective average Q^2 for each detector to better than 3%.

11.4 Projected results

Since the solid angle of this spectrometer is 5 times smaller than the HMS, but the integrated luminosity is 5 times larger with GEP-III than that requested for the HMS option (corrected for the difference in average Q^2), the statistical error on LH2 will be very similar the HMS option. One difference is that both the low and high Q^2 settings will be on LH2, while with HMS only LD2 will be studied at low Q^2. The W region that can be covered is slightly larger than with two HMS settings, and the W resolution is very similar to the HMS option (see Fig. 8). The two average Q^2 values using $E = 6$ GeV are not as spread apart: 0.6 and 0.9 GeV^2, compared to 0.5 and 1.0 GeV^2 with the HMS. On the other hand, some additional data at low Q^2 will be obtained from the 20 days of GEP-III+ running at energies below 6 GeV. There would be no results for A_d, since GEP-III+ is only running with LH2. The systematic errors are all very similar to that for the HMS, with the exception of the estimated error on the average Q^2. Because the Q^2 range is much larger with the parasitic spectrometer, and because the HMS has a much better understood acceptance, we estimate the overall systematic error on A_p to be 3% from the uncertainty in average Q^2. Background levels in the lead glass are likely to be bigger as well. The resulting systematic error is hard to quantify until the actual background levels are measured.

11.5 Impact

Unlike the HMS option, which requires only a minor hardware change, the parasitic spectrometer option requires approximately one month of setup time in the hall, and a small amount of extra capital equipment money for detector stands, cables, etc. The electronics cost is the same for both options. Additional lab resources would be needed for making new pole pieces for the splitter magnet, and for magnetic field mapping. Finally, the electricity bill for running the three magnets for four months is not negligible (about 3 GW-hrs).

11.6 Comparison to HMS option

The main advantages of the GEP-III+ parasitic option are that it takes 9 less days of dedicated beam time, and it would be run relatively soon.

The main drawbacks are

- Substantial time needed for design, engineering, and setup. The impact on running time would depend on the scheduled length of the down time prior to GEP-III+.
- Larger detector backgrounds (hard to quantify).

- Larger systematic error in average Q^2 leading to an overall increase in total systematic error of about 60%.
- Only LH2 would be run

References

[1] C.Y. Prescott *et al.,* Phys. Lett. 77B, 347 (1978); 84B, 524 (1979).

[2] NuTeV Collaboration, G.P. Zeller *et al.*, Phys. Rev. Lett. 88 (2002) 091802. Minor revisions in hep-ex/0110059 v.3 (2003) and hep-ex/0203004 v.3 (2003).

[3] Particle Data Group, Phys. Rev. D 66, (2002) 010001.

[4] SLAC E158 Collaboration, P.L. Anthony *et al.*, Phys. Rev. Lett. 92, 181602 (2004).

[5] A. D. Rujula, H. Georgi and H. D. Politzer, Ann. Phys. 103, 315 (1977).

[6] E. D. Bloom and F. J. Gilman, Phys. Rev. Lett. 25, 1140 (1970).

[7] I. Niculescu *et al.*, Phys. Rev. Lett. 85, 1186 (2000).

[8] C. E. Carlson, N. C. Mukhopadhyay, Phys. Rev. Lett. 74, 1288 (1995).

[9] A. Bodek, I. Park, and Un-ki Yang, hep-ph/0411202 (2004).

[10] J.E. Amaro, M.B. Barbaro, J.A. Caballero, T.W. Donnelly, A. Molinari, Physics Reports 368, 317 (2002); M.B. Barbaro, J.A. Caballero, T.W. Donnelly, A. Molinari, Phys. Rev. C69, 035502 (2004); A. De Pace, M. Nardi, W.M. Alberico, T.W. Donnelly, A. Molinari, Nucl. Phys. A741, 249 (2004).

[11] M.J. Musolf *et al.*, Phys. Rept. 239, 1 (1994)

[12] R. Cahn and F. Gilman, Phys. Rev. D17, 1313 (1978).

[13] D.R.T. Jones and S.T. Peteov, Phys. Lett. B91 (1980) 137; L.M. Nath, K. Schilcher, M. Kretzschmar, Phys. Rev. D 25 (1982) 2300.

[14] G. F. Sacco, Ph.D. Thesis, University of Connecticut, 2004 (unpublished).

[15] J. Blumlein *et al.,* HERA Workshop Vol. 1, p. 69, Hamburg 1989.

[16] J. Erler and P. Langacker, Particle Data Group, Phys. Rev. D 66, (2002) 010001.

[17] S.L. Adler, Ann. Phys. 50 (1968) 189.

[18] C. E. Keppel, in proceedings of the SPIN 2002 conference, 2002, New York.

[19] F. Close and N. Isgur, Phys. Lett. B509, 81, 2001.

[20] W. Melnitchouk, R. Ent, C. E. Keppel, to be published in Rev. Mod. Phys.

[21] Y.S. Tsai, Report No. SLAC-PUB-848, 1971; Rev. Mod. Phys. 46 (1974) 815.

[22] D.Y. Bardin *et al.,* Yad. Phys. 29 (1979) 499; Nucl. Phys. B 197 (1982) 1.

[23] Shi-Lin Zhu, C.M. Maekawa, G. Sacco, B. R. Holstein,, M.J. Ramsey-Musolf, Phys. Rev. D65 (2002) 033001.

[24] D.E. Wiser, Ph.D thesis, U. Wisconsin, 1977 (unpublished).

[25] S-P. Li, E.M. Henley and W-Y.P. Hwang, Annals of Physics 143 (1982).

[26] S.L. Zhu, C.M. Maekawa, B.R. Holstein and M.J. Ramsey-Musolf, Phys. Rev. Lett. 87 (2001) 201802.

[27] T. Sjostrand, Computer Physics Commun. 82, 74 (1994).

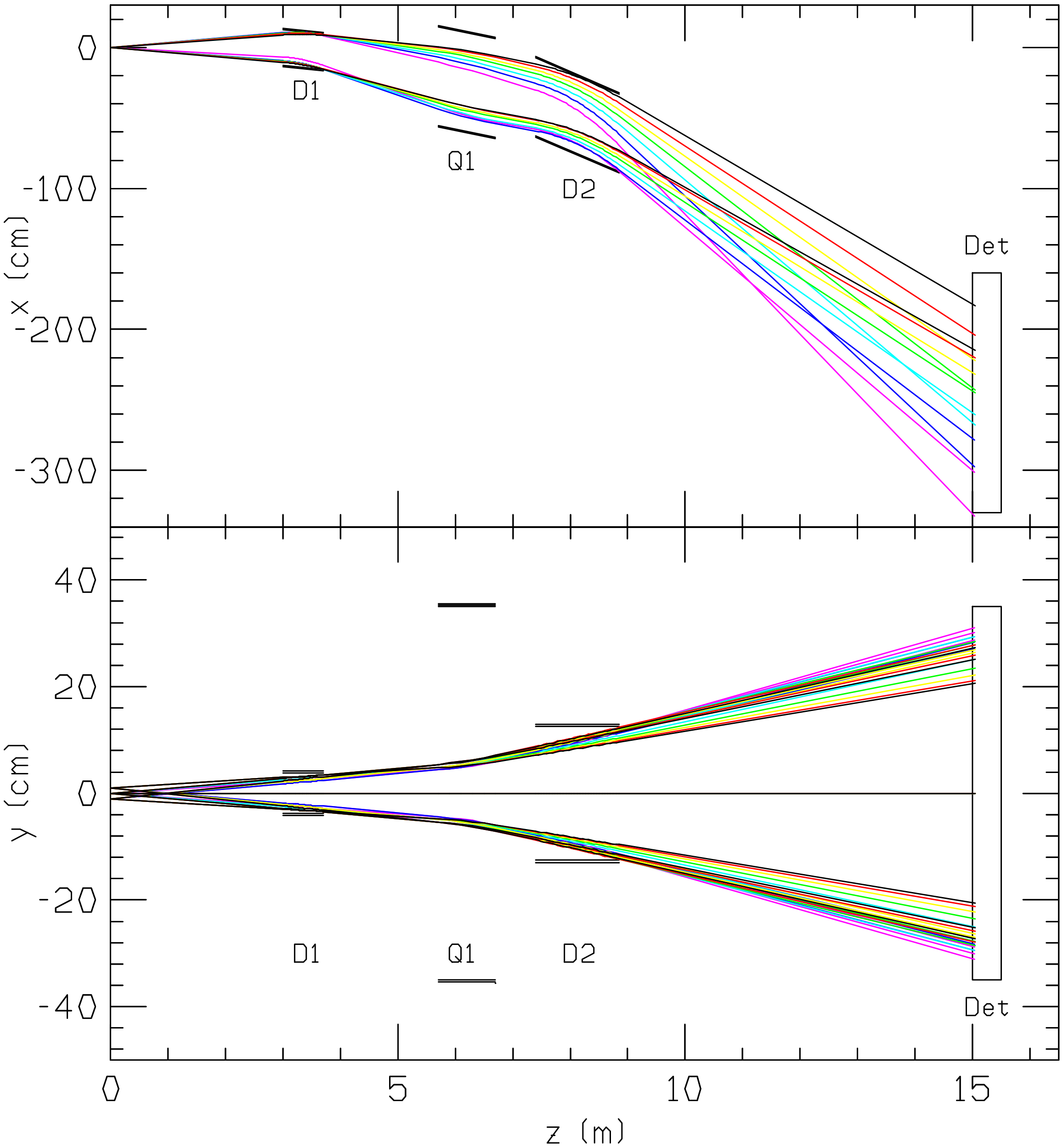

Figure 6: Optical raytrace for the Res-Parity spectrometer. The top plot shows the horizontal view (from below), with the different colors representing different values of constant W spanning the region $1 < W < 2.2$ GeV. The lower plot shows the vertical view.

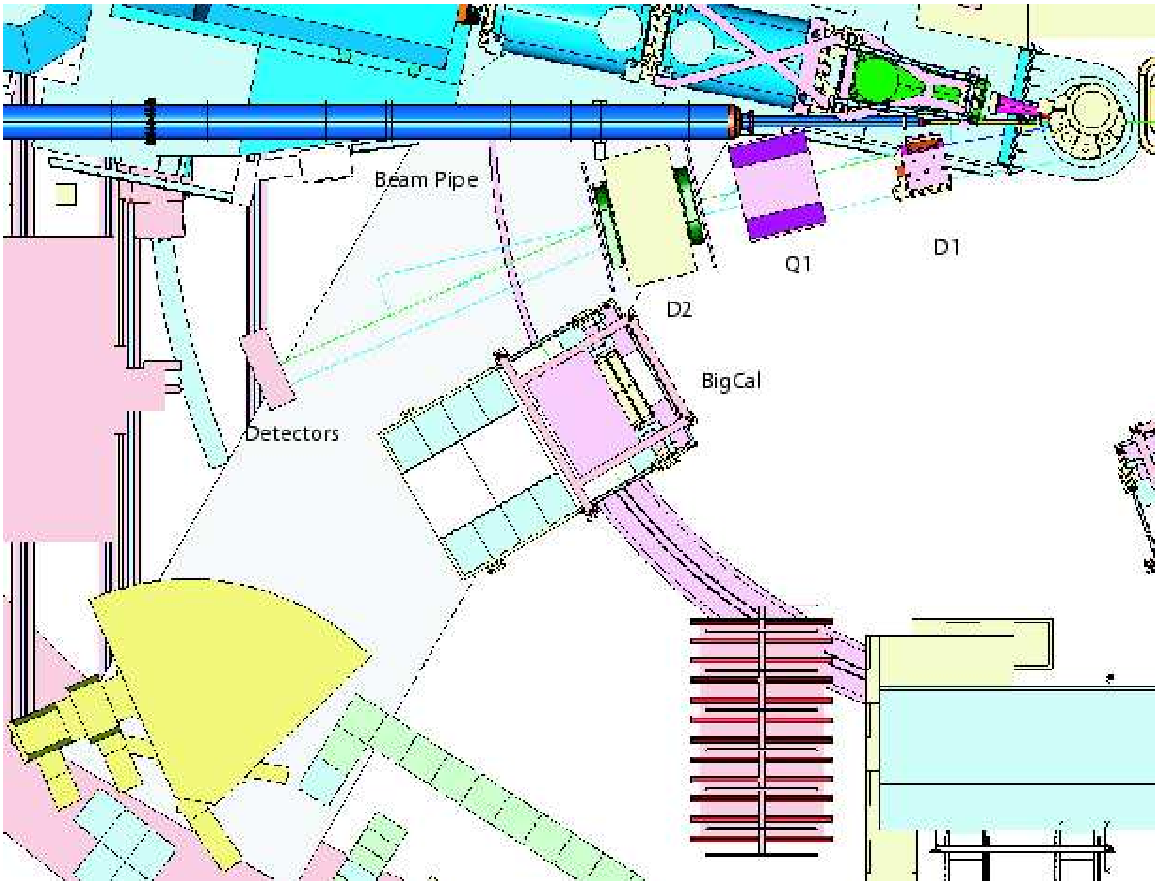

Figure 7: Layout of the Res-Parity spectrometer in Hall C, located just below the beam line. Also shown is the beam pipe and the Big-Cal detector for GEP-2γ at the smallest angle of that experiment.

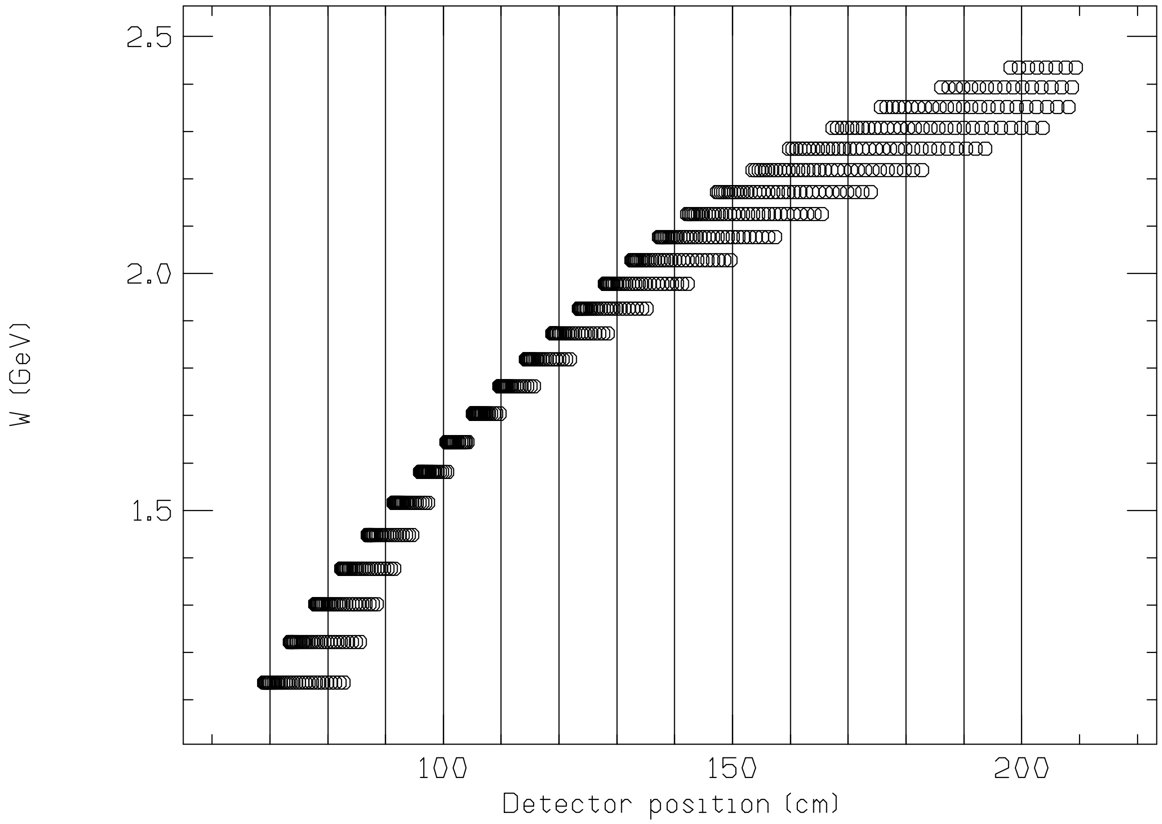

Figure 8: Missing mass W as a function of detector position for the Res-Parity spectrometer. The vertical bars indicate the 10 cm spacing of the lead glass blocks.